Check for updates

Facile one-step fabrication of upconversion fluorescence carbon quantum dots anchored on graphene with enhanced nonlinear optical responses

Chan Zheng, [ID] *[ab] Li Huang,[a] Qiaohang Guo,[ab] Wenzhe Chen,[a] Wei Li[ab] and Haiyan Wang[a]

A novel nanocomposite hybrid, carbon quantum dots (CQD)/graphene oxide (GO), which combines the favorable optical properties of both its components, is synthesized by a facile one-step electrochemical method. Transmission electron microscopy, Raman spectroscopy, UV-vis spectroscopy, and fluorescence studies show that the CQDs uniformly attach on the GO surface, which enables highly efficient energy transfer between CQDs and GO. The nonlinear optical and optical limiting (OL) performances are investigated by the open-aperture *Z*-scan technique in the nanosecond regime using a laser with a wavelength of 532 nm. The as-prepared CQD/GO composite offers a significantly improved OL performance compared with GO because of the charge/energy transfer process between the CQDs and GO. The main contributors to the enhanced OL effect in the CQD/GO hybrid are a combination of nonlinear scattering and increased nonlinear absorption resulting from efficient charge/energy transfer at the CQD/GO interface.

1. Introduction

Since the appearance of the first operational laser in 1960, new and improved laser technology for both civilian and military purposes has continued to be at the forefront of research worldwide, owing to the coherent, monochromatic, and single-directional properties of laser light. However, the potential damage caused by lasers to the human eye and to precise optical instruments has become increasingly apparent, greatly stimulating the development of laser protection materials. Much effort has been invested into research into smart materials and processes over the past decades in an attempt to afford some measure of protection from laser beams. Optical limiting (OL), an important application of nonlinear optics (NLO), useful for the protection of the human eye, optical elements, and optical sensors from intense laser pulses, is of great interest to private industry, law enforcement, and the military. A good optical limiter is a material that allows optical radiation to pass through at low fluences but suppresses the transmitted intensity as the laser fluence increases. Materials with this property can be useful to fabricate devices for pulse shaping,[1] passive mode locking,[2] and eye protection against powerful lasers.[3]

Extensive research has been performed on optical limiters in the past 20 years, and the strong OL properties of a wide range of materials have been intensively studied, from organic dyes (phthalocyanine, porphyrin, fullerene),[4–9] carbon nanomaterials (carbon black, carbon nanotubes, graphene)[10–15] to noble metal nanoparticles (NPs)[16–18] and quantum dots.[19–21] Typically, the occurrence of OL effects in materials arises from three main classes of mechanisms: nonlinear absorption (NLA), nonlinear scattering (NLS), and nonlinear refraction (NLR).

Despite significant progress in the past decade in the development of NLO nanomaterials and their nonlinear interaction with light, no one individual OL material can effectively fulfill all the requirements of ideal OL materials, including broadband effectiveness, rapid limiting response, low limiting threshold, and high damage threshold. Therefore, there is still an urgent need for highly NLO-responsive components. Of particular interest are hybrid nanomaterials, which offer a new and convenient basis for novel NLO components that interact strongly with ultrafast laser pulses.[22–28] Compared with their individual constituents, hybrid nanomaterials often exhibit enhanced NLO effects and/or flexible processability,[22–28] resulting from the unique structures and synergistic coupling effects between the constituents.

Recently, graphene and its derivatives have been shown to be ideal substrates to synthesize multicomponent materials because of their large 2D aromatic surfaces, especially when the surfaces are functionalized with oxygen-containing groups,

[a]*School of Materials Science and Engineering, Fujian University of Technology, 3 Xueyuan Road, Fuzhou 350108, P. R. China. E-mail: czheng.fjut@gmail.com*

[b]*Fujian Provincial Key Laboratory of Advanced Materials Processing and Application, 3 Xueyuan Road, Fuzhou 350108, P. R. China*

such as hydroxyl and epoxide moieties. These groups can act as reactive sites for chemical modification using recognized carbon surface chemistry.[29–31] To date, graphene-based composites have been successfully synthesized from inorganic nanostructures, organic crystals, polymers, metal–organic frameworks, biomaterials, and carbon nanotubes, and have been intensively explored in applications such as batteries, supercapacitors, fuel cells, photovoltaic devices, photocatalysis, sensing platforms, and Raman enhancement.[29–31] Most importantly, because of their ultrafast carrier dynamics and good incident-light absorption capabilities, nanocomposites based on graphene and its derivatives have become the benchmark for broadband optical limiters, outperforming their single-component equivalents.[24–28] Particularly, recent results indicate that such nanocomposites show improved NLO or OL properties compared with those of the individual components. As a result, great progress has been achieved in the loading of single materials, including metal NPs, metal oxide NPs, quantum dots, phthalocyanines, and porphyrins, onto graphene surfaces to obtain composites for NLO and OL applications.[24–28]

At the same time, carbon quantum dots (CQDs) have emerged as a particularly interesting carbon nanomaterial. These have drawn considerable attention owing to their unique properties, including excellent chemical and photostability, biocompatibility, easy functionalization, and upconversion of photoluminescence. These features have been applied in fields such as bioimaging, solar light harvesting, chemical and biochemical analysis, photocatalysis, and optoelectronics.[32–34] Notably, CQDs have recently been shown to exhibit excellent NLO and OL responses[35–38] and exhibit considerable third-order NLO responses comparable to C_{60}, a well-known form of molecular carbon with proven NLO properties. However, to the best of our knowledge, although some groups reported the preparation of CQD/GO hybrid,[39] no studies reported the NLO and OL performances of nanocomposites of CQDs and graphene oxide (GO). This design strategy could potentially generate superior OL performance by combining the advantages of both carbon-based nanomaterials, thus enabling development of multifunctional carbon-based OL materials and providing new insight into the development of novel nano-architectures with versatile properties.

In the present work, a nanohybrid with ultrafine and well-dispersed CQDs supported on GO nanosheets, which combines the favorable optical properties of CQDs and graphene phases, is synthesized by a one-step electrochemical method. Electrochemistry allows control over the product's electronic states via adjusting the external power source to change the Fermi energy level of the electrode material's surface. For the first time, we report a facile and rapid approach to the synthesis of ultrafine and well-dispersed CQDs decorated on GO nanosheets at a graphite electrode under aqueous solution. Transmission electron microscopy (TEM), atom force microscopy (AFM), Raman spectroscopy, ultraviolet–visible (UV-vis) absorption spectroscopy, and photoluminescence (PL) spectroscopy were used to elucidate the surface morphologies, structures, and linear optical properties of the obtained CQD/

GO nanohybrids. The NLO and OL performance of CQD/GO were characterized by the Z-scan technique using 532 nm laser pulses with a pulse duration of 4 ns. The CQD/GO hybrids showed stronger NLO and OL effects for nanosecond laser pulses at 532 nm than did the individual GO. The possible mechanisms are also discussed.

2. Experimental

2.1 Synthesis of the CQD/GO hybrid nanostructures

The CQD/GO nanocomposites were synthesized by a facile electrochemical method. Typically, a graphite rod (99.99%, Alfa Aesar Co. Ltd.) was inserted into ultrapure water as the anode (18.4 MΩ cm^{-1}, 500 mL), which was placed parallel to another graphite rod as the counter-electrode with a separation of 5.0 cm. Static potentials of 30 V were applied to the two electrodes using a direct current (DC) power supply. After continuous stirring for 120 h, the CQD/GO hybrid was obtained, the anode graphite rod became corroded, and a solution appeared gradually in the reactor. The solution was centrifuged to remove the precipitated graphite oxide and graphite particles, and filtered and dialyzed with a cellulose ester membrane bag [MD77 (8000 – 14 000)]. The solution was dialyzed and finally concentrated to be characterized. For comparison, GO was prepared by oxidizing natural graphite powder via the modified Hummers method.[40] Individual CQDs were prepared by hydrothermal synthesis using heparin sodium as a raw material. A 40 mL portion of 0.0275 g mL^{-1} sodium heparin solution was added to a 50 mL stainless-steel autoclave and reacted in an oven for 12 h at 140 °C. The reacted black mixture was filtered and the filtrate was centrifuged at 10 000 rpm for 10 min at 23 °C. After vacuum filtration (filter membrane: 0.22 μm) and dialysis (MWCO = 3500/8000) a light brown supernatant was obtained. The dialyzed solution was then dried in a drying air oven for 48 h (60 °C) to obtain a concentrated CQD solution. The solution was further dried to obtain the CQD powder.

2.2 Characterization

The morphology of the CQD/GO hybrids was investigated by TEM (JEM-2010, accelerating voltage 200 kV). The samples were ultrasonicated in ethanol to ensure dispersion. A drop of the dispersed sample was left to dry on a commercial carbon-coated Cu TEM grid. AFM measurements were performed on a Dimension Icon (Bruker Nano) AFM. About 0.5 μL CQD/GO solution was spotted onto a cleaned silicon wafer and dried in a vacuum oven (~12 h, 50 °C). Samples were imaged in air by tapping-mode AFM on a Nanoscope Vcontroller with HAR1-200-10 tips (silicon cantilever, Bruker AFM Probes). The tip–surface interaction was minimized by optimizing the scan set point. Raman spectra of the CQD/GO hybrid composites were obtained using a Raman spectrometer (Renishaw Invia) at ambient temperature with an excitation wavelength of 514.4 nm. UV-vis spectra were recorded using a UV-vis spectrophotometer (UV-2600). The absorption behavior of the CQD/GO suspensions was measured in quartz cells with a path length of 10 mm. The fluorescence properties of the samples were

measured with an FM-4 fluorescence spectrometer (HORIBA Jobin Yvon, France).

2.3 *Z*-scan measurements

The NLO and OL behavior of the CQD/GO hybrids was investigated by the open-aperture (OA) *Z*-scan technique.[41] The excitation light source was a Nd:YAG laser (Brio 640, Quantel, Les Ulis, France) with a repetition rate of 1 Hz. The laser pulses (period 4 ns, wavelength 532 nm) were split into two beams by a mirror. The pulse energies at the front and back of the samples were monitored using energy detectors (PE25, Ophir Optronics Solutions Ltd., Jerusalem, Israel). The beam waist at the focus is 14.5 μm, and thus the Rayleigh length is 1.24 mm. The energy of a single pulse was 120 μJ and the peak intensity at the focus calculated to be 8.53 GW cm^{-2}. All of the measurements were performed at room temperature. The samples were dispersed in ethanol and added to 1 mm-thick glass cuvettes. The cuvettes were mounted on a computer-controlled translation stage that shifted the samples along the *z* axis. An error of ±5% in the transmittance data has been observed during the measurement of far field transmittance by the detector.

3. Results and discussion

3.1 Morphology and structure characterization

The success of the one-step electrochemical strategy to produce CQD/GO hybrids was confirmed by the TEM images. The representative TEM images in Fig. 1 show the synthesized samples of CQD/GO hybrid. As shown in Fig. 1(a) and (b), the ultrafine and uniform CQDs with sizes of approximately 5 nm were homogeneously anchored on a two-dimensional GO sheet. As revealed in the HRTEM images (Fig. 1(c) and (d)), the lattice spacings of graphene and CQDs are about 3.41 and 2.08 Å, respectively, corresponding to the (002) plane of crystalline graphite and (100) spacing of single carbon dots. To obtain more insight into the size of the CQDs on the surface of GO, AFM images were recorded. Fig. 1(e) and (f) confirms the dispersed graphene to be wrinkled sheets with an average height of 6.24 nm, implying that the average size of the anchoring CQDs is also approximately 6.24 nm. The TEM results clearly confirmed that the CQD/GO hybrid was successfully synthesized using a facile electrochemical method.

The formation mechanism of CQD/GO hybrids is worth further exploring. The composites were synthesized through a mild, one-step electrochemical approach, in which only pure water is used as the electrolyte and graphite rods as both anode and cathode. Graphite is a layered crystal formed by the stacking of carbon hexagonal symmetry planes. The carbon atoms are covalently bonded to each other in each layer, while the layers are combined through van der Waals forces. Therefore, it can be imagined that judicious cutting of a graphite honeycomb layer into ultra small particles can lead to tiny fragments of graphite, yielding CQDs and/or graphene. During constant voltage electrolysis, cations (H$^+$) and anions (OH$^-$) of the electrolyte move toward the cathode and the anode, respectively. Under an electric field, ions would enter the graphite sheets to increase the spacing between the graphite layers, thus weakening the interaction force between the layers. With the electrolysis reaction processed, the graphite on the cathode electrode is continuously corroded, and the surface of the electrode expanded obviously. It also can be seen that some colored materials were shed on the surface of the electrode, and the stripped graphite layers (including CQDs, GO, and graphite sheet) appeared in the electrolyte. The resulted solution was centrifuged to remove the precipitated graphite oxide and graphite particles, and filtered and dialyzed with a cellulose ester membrane bag to obtain CQD/GO hybrid.

Raman spectroscopy is an effective method to characterize carbon-based materials. Raman spectra contain information on the chemical environment of the sp^2 and sp^3 carbon atoms in graphite, diamond, fullerene, carbon nanotubes, graphene, and other carbon materials, and allow their structural features to be characterized. Fig. 2 indicates the Raman spectra of GO and the CQD/GO hybrid, illustrating the influence of the decorating CQDs on the structure of GO. The spectra of the graphene-based nanostructures contain two characteristic peaks in the range 500 to 3500 cm^{-1}, termed the G band and D band, respectively. The D band is a breathing mode of the κ-point phonon with A$_{1g}$ symmetry. This peak mainly originates from lattice defects, such as vacancies, edge crimping, and sp^3-hybridized carbon atoms linked to the oxygen-containing groups. The G band is associated with the E$_{2g}$ phonons of the sp^2-hybridized carbon atoms. The broad and symmetrical 2D band in the region of 2700–3100 cm^{-1} indicates that the CQD/GO is highly oxidized and consists of only a few layers. Generally, the intensity ratio of the D peak to the G peak (I_D/I_G) is used as an indicator of the level of functionalization. The I_D/I_G ratios for GO and CQD/GO are 1.05 and 1.09, respectively. The negligible change of the ratio indicates the restoration of the original sp^2 network on the surface of GO after the introduction of CQDs.

3.2 Linear optical properties

The linear optical properties of the CQD/GO composite nanostructure were studied by UV-vis and PL spectroscopy. The UV-vis absorption spectra of the GO and CQD/GO hybrid in aqueous solution are presented in Fig. 3. As can be seen, GO displays one well-defined absorption peak at around 230 nm and a shoulder centered at 300 nm. The former is attributed to the π → π* transition of aromatic C=C bonds, resulting from the highly conjugated aromatic structure, while the latter can be ascribed to the n → π* transition of C=O bonds. After the assembly of CQDs on the GO, the characteristic absorption of GO became even weaker and broader as a result of an interparticle coupling effect. Meanwhile, the absorption peak at 230 nm has slightly narrowed down in case of CQD/GO composite probably due to the fact that attaching with CQDs inhibits the π → π* transition of aromatic C=C bonds. The absorption spectrum of CQD/GO did not show any new absorption characteristics, indicating that no charge diffusion or electronic interaction occurred between the CQDs and GO in their ground state. In addition, the C–O and C=O bonds indicate the presence of a large number of oxygen-containing
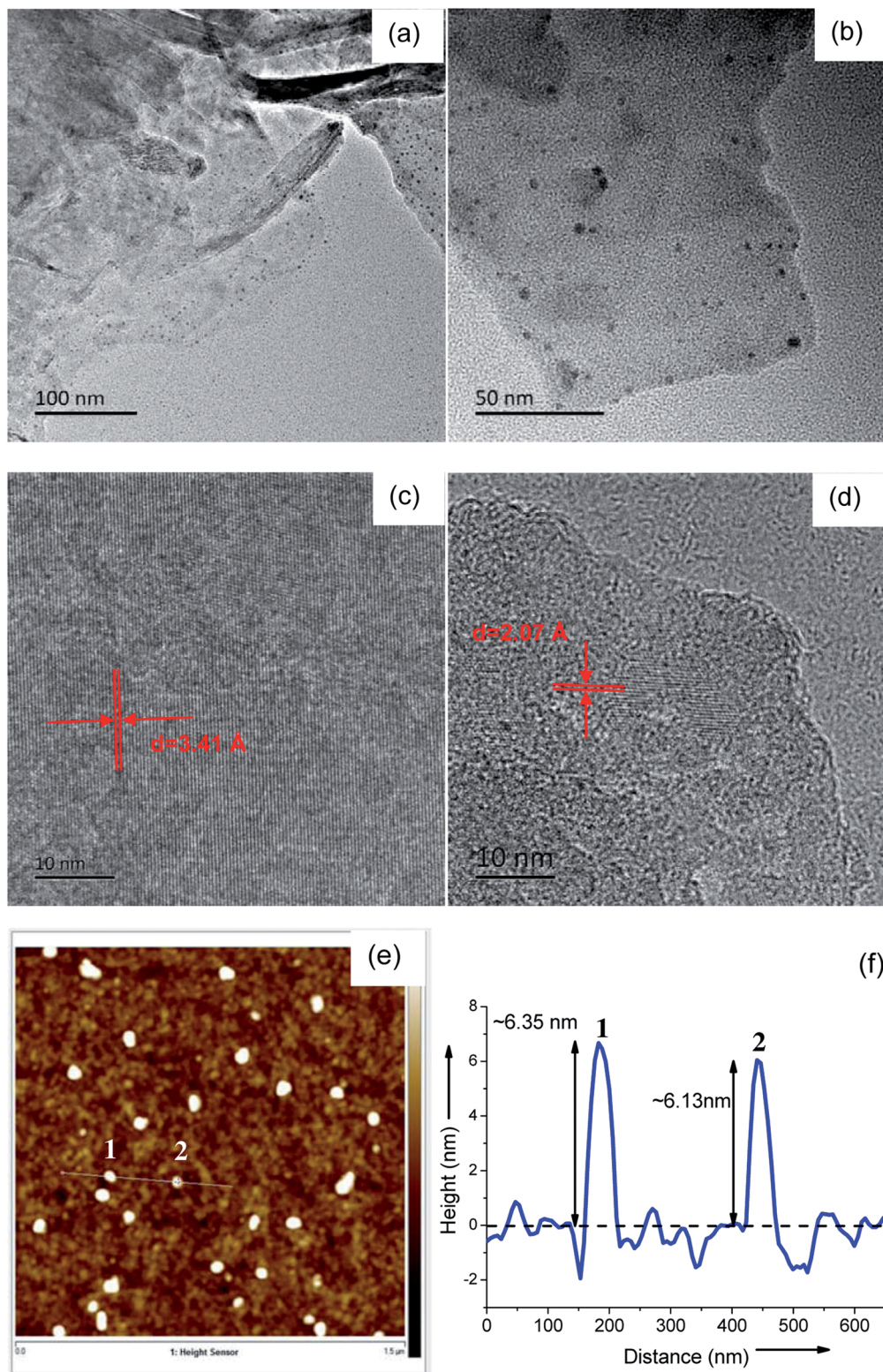
Fig. 1 (a) and (b) TEM images of CQD/GO. (c) and (d) HRTEM images of CQD/GO. (e) AFM image of CQD/GO on a silicon substrate. (f) The corresponding height-profile along the line in (e).

groups (such as hydroxyl, carboxyl, carbonyl, and epoxy) on the GO and CQD/GO hybrid.

To further explore their linear optical properties, the GO, CQDs and CQD/GO hybrids were studied by PL spectroscopy.

The PL data in Fig. 4(a) show that the GO emitted a broad band centered at around 430 nm. Because of the wide size distribution of sp^2 domains in GO, which calculated to be 4.19 nm from Raman data,[42] the corresponding band gaps also cover a wide
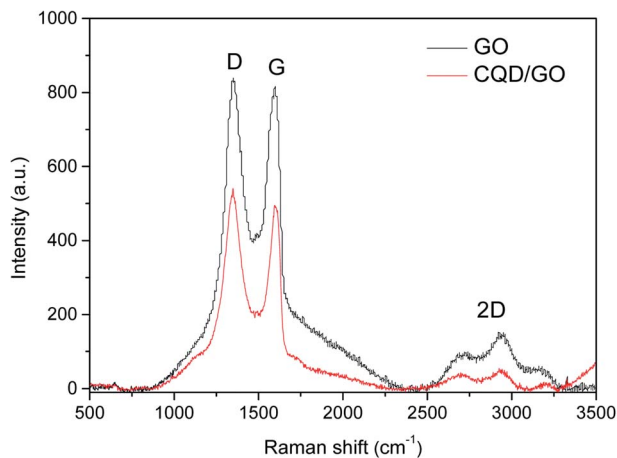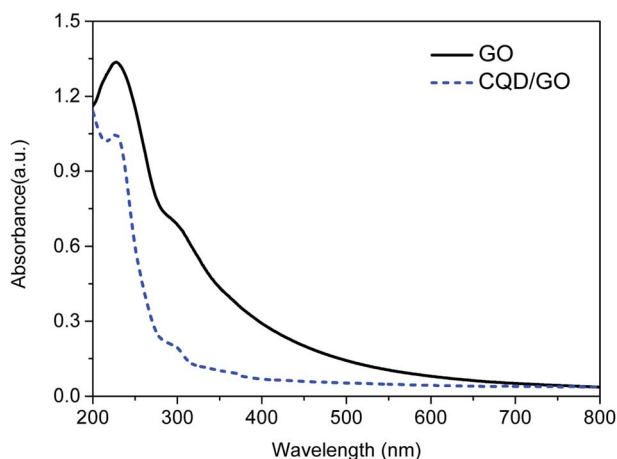
Fig. 2   Raman spectra of GO and CQD/GO hybrid.

Fig. 3   UV-vis spectra of GO and CQD/GO in aqueous solution.

Fig. 4   (a) PL spectra (λ_{ex} = 320 nm) of CQDs, GO and CQD/GO in aqueous solution at room temperature. (b) PL spectra of CQD/GO hybrid at different excitation wavelengths.

size range, leading to a wide PL emission spectrum from visible to near infrared. Upon excitation at 340 nm, the CQDs exhibit one broad and strong emission band at around 450 nm (Fig. 4(a)). This is caused by both an intrinsic band gap, resulting from confined sp^2 conjugation in the core of the CQDs, and extrinsic fluorescence, resulting from a surface state that can be excited either directly or by energy transfer from an intrinsic band. It is clear that the characteristic emission of the CQDs between 350 and 650 nm was dramatically reduced after attachment to the GO, suggesting a strong PL quenching effect in the CQD/GO hybrid. Previous studies found that GO likewise possesses a similar quenching efficiency against inorganic QDs and fluorescent dyes.[42] In the current study, energy transfer is one of the possible mechanisms for PL quenching in the CQDs. It is known that PL emission originating in CQDs can be effectively quenched by both electron donors and acceptors. Therefore, the observation of quenching here indicates that efficient charge/energy transfer occurs at the CQD/GO interface. The transferred energy is accepted by GO, which therefore displays enhanced PL intensity. In addition, the emission band is slightly red-shifted in the CQD/GO hybrid, which results from an increase in surface defects on the GO surface after
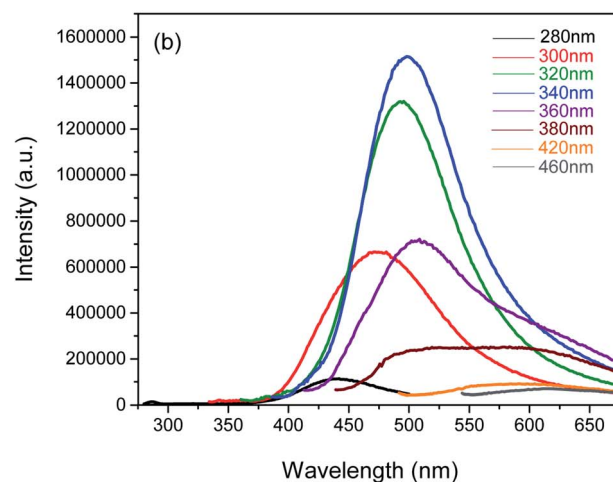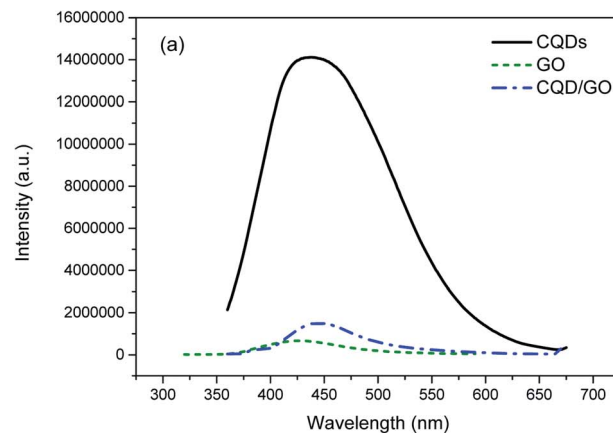
modification by the attachment of CQDs. The excitation-dependent emission, *i.e.*, PL maximum of CQDs has been widely reported to red-shift as the excitation wavelength increases.[43,44] Interestingly, the PL emission in the CQD/GO hybrid also displayed such excitation-wavelength-dependent PL behavior, as shown in Fig. 4(b). The efficient charge/energy transfer from the CQDs to the GO highlights the potential for CQD/GO to behave as an effective light conversion device.

3.3   Nonlinear optical performance

Carbon-based materials, including fullerenes, carbon nanotubes, graphene, and carbon black nanoparticles, often exhibit strong NLO properties, which has led to pronounced interest in these materials with regard to the realization of NLO devices, such as optical limiters. In addition, based on the results discussed above, an improved NLO and OL effect should be expected from the CQD/GO hybrid, compared with that of GO, because of the charge/energy transfer between the decorated species and substrate GO. The OA Z-scan technique was employed in the present study to investigate the NLO and OL responses in the nanosecond regime at 532 nm. The sample concentrations were adjusted to obtain a uniform linear transmittance of 80% at 532 nm in 1 mm-thick cells using a UV-vis

spectrometer to ensure equivalent absorbance. The OL effects of the samples, manifested by plotting the normalized transmittance *versus* the input energy density, were calculated from the OA *Z*-scan measurements, as illustrated in Fig. 5. The OL property of pure aqueous was also measured at the same conditions to clarify the solvent contribution. In the pure aqueous, we has not observed an OL effect at 532 nm, the major contribution of OL arises from the CQD, GO, and CQD/GO hybrid. All of the samples present a similar trend, that is, the transmittance remains constant at low input fluence and then decreases as the fluence increases beyond a threshold value. This is a typical feature of OL materials, indicating that all three samples are potential OL candidates. The OL threshold (defined as the input fluence at which the transmittance falls to 50% of the linear transmittance) was determined to be larger than 3 J cm^{-2} for CQDs and GO, 2.15 J cm^{-2} for CQD/GO, respectively. This shows that the anchored CQDs helped to enhance the OL performance of GO by lowering the OL threshold, which verifies the superior performance of the composite system.

Several mechanisms have been found to be responsible for the OL behavior of different materials, specifically, NLA (two-photon absorption (2TA), free-carrier absorption, and reverse saturable absorption), NLS, and NLR. CQDs exhibit similar properties to other species of quantum dots. Therefore, the origins of their NLO response can be assumed to be similar to those of their inorganic counterparts. For QDs, the generally accepted underlying OL mechanisms are two-photon and/or multiphoton absorption for pico- to femtosecond laser pulses and free-carrier absorption and/or NLS for nanosecond laser pulses.[19–21,35–38] By the closed-aperture *Z*-scan techniques, which can conveniently and effectively distinguish between NLA and NLR, it was confirmed that NLR made no contribution to the observed NLO and OL behavior of the CQD/GO hybrid in response to nanosecond laser irradiation in our experiments. To separate the contributions of NLA and NLS, we used a *Z*-scan setup following Joudrier and Rao[45,46] and the results are shown in Fig. 6. The intensity variation along the beam propagation

direction z in a medium having a third-order nonlinearity is described as $\mathrm{d}I/\mathrm{d}z = -\alpha_0 I - \alpha_2 I^2$, where α_0 is the linear absorption coefficient, and α_2 is the total nonlinear extinction coefficient. The coefficient α_2 is a sum of contributions from both NLA (α_{2A}) and NLS (α_{2S}): $\alpha_2 = \alpha_{2A} + \alpha_{2S}$. The position-dependent transmittance (the "*Z*-scan curve") is given by:[41]

Fig. 5 Normalized transmittance OL curves of GO and CQD/GO samples in aqueous solution at 532 nm. The linear transmittance of each sample was individually adjusted to 80%.
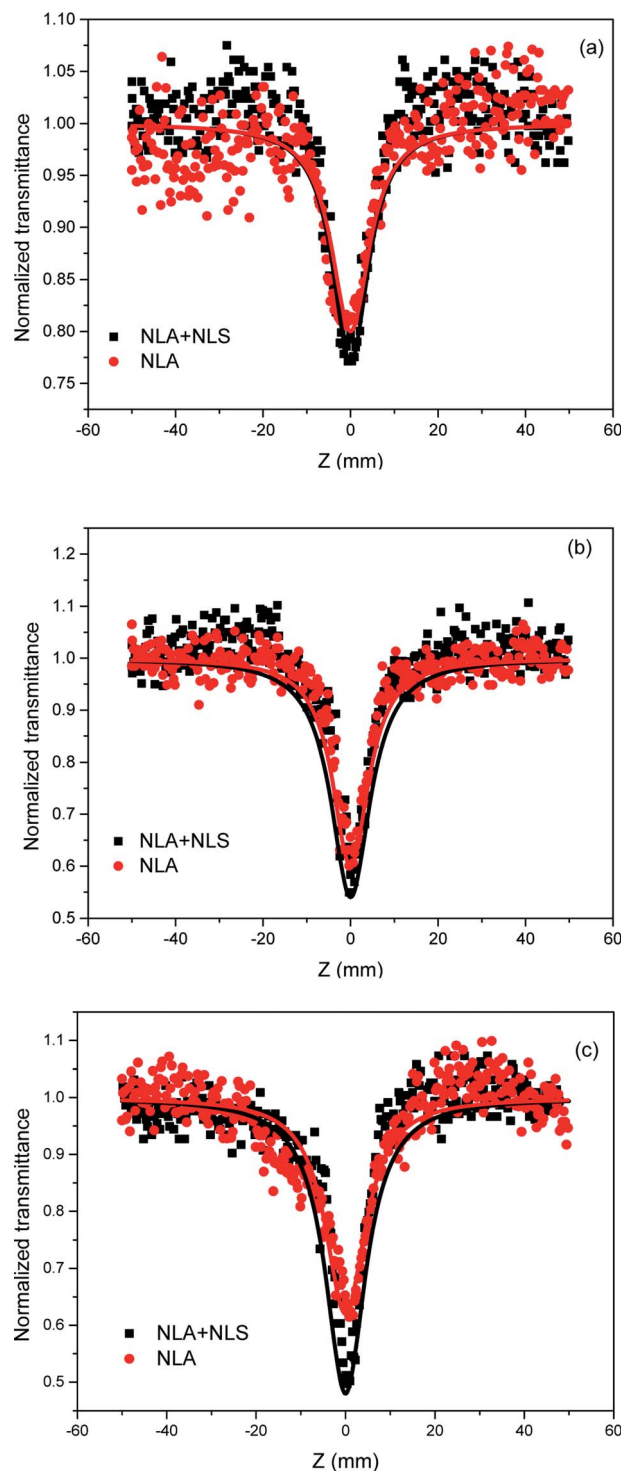

Fig. 6 OA *Z*-scan curves of (a) CQDs, (b) GO and (c) CQD/GO samples in aqueous solution at 532 nm. The linear transmittance of each sample was individually adjusted to 80%.
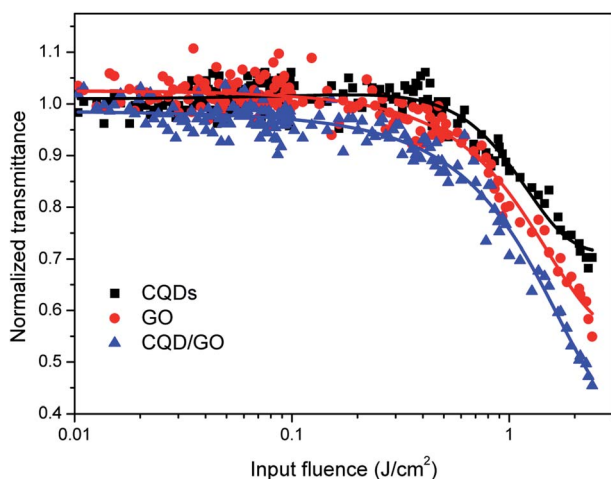
$$T(z) = \left[1/\pi^{1/2}\right] \int_{-\infty}^{\infty} \ln[1 + q_0(z)\exp(-\zeta)]\mathrm{d}\zeta \qquad (1)$$

where z is the sample position with respect to the focus and $q(z) = \alpha_2 I_0 L/[1 + (Z/Z_0)^2]$, with I_0 being the peak intensity at the focal point. L is the effective length of the sample, given by $[1 - \exp(\alpha_0 l)/\alpha_0]$, where l is the sample length, and $Z_0 = \pi\omega_0^2/\lambda$ is the Rayleigh range, where ω_0 is the beam waist radius at the focus and λ is the wavelength of the light. The value for α_2 is obtained by fitting the $T(z)$ equation to the experimental data. In the context of our experiment, i.e., the Z-scan in Fig. 6, curve (b) gives α_2, and curve (a) is fitted with α_{2A}. The error incorporated during the fitting of the experimental points with eqn (1), has been estimated are included in the values of α_2, α_{2A}, and α_{2S}. Thus, the values of α_2, α_{2A}, and α_{2S} were calculated to be 0.99 ± 0.05, 0.81 ± 0.04, and 0.18 ± 0.01 for the CQDs; 1.68 ± 0.08, 1.59 ± 0.08, and 0.09 ± 0.01 for GO; and 2.16 ± 0.11, 1.59 ± 0.08, and 0.57 ± 0.03 ($\times 10^{-11}$ cm W^{-1}) for the CQD/GO hybrid. It is clear that except for NLA, NLS makes a contribution to the total extinction in the GO and CQD/GO hybrid.

The enhanced NLO and OL performances of the CQD/GO hybrid can be further understood in terms of a process by which laser pulses promote electron and/or energy transfer from the electron donor, i.e., ultra-small CQDs, to the electron acceptor, GO. The origins of the observed OL behaviors of the CQDs can be attributed to free carriers. The electrons from the valence band can be excited to the intermediate states of the linear absorption tail through inter-band transitions, leading to the generation of a large number of free carriers when excited by laser pulses. These free carriers can be further excited to higher levels in the conduction band by absorbing photons (intra-band transitions), giving rise to NLA. Meanwhile, GO, possessing a highly delocalized conjugated structure and superior electrical conductivity, can efficiently transfer the photo-generated free carriers, which suppresses the charge recombination and produces a charge-separated excited state, leading to the enhanced NLO and OL response in the CQD/GO hybrid.

In addition, the enhancement of NLS also contributed to the improved OL activities in CQD/GO hybrid. Generally, NLS may play the most important role in the OL behavior of nanomaterials. Thermal induced NLS scattering centers consist of two origins: the formation and growth of solvent bubbles and the formation and expansion of microplasmas. The former takes place at the lower incident energy fluence, while the latter takes place at higher fluence. Although nanoscale particles cannot effectively scatter the laser beam according to the Mie scattering theory because of the small size of the scattering centers, the NLS of the CQD/GO hybrid clearly outperforms those of the GO sample, indicating the enhanced NLS induces by the anchoring CQDs. When irradiated by ns laser pulses, light absorption by CQDs and GO induces a enhanced temperature in the nanostructures, which leads to formation of rapidly expanding microplasmas. Formation and rapid expansion of these microplasmas then transfers thermal energy to the surrounding medium, forming solvent microbubbles. When the size of the bubbles increases to the magnitude of the incident light wavelength, the bubble clouds effectively scatter the

incident beam, realizing reduction of transmission. These microplasmas and microbubbles strongly scatter light from the transmitted beam direction, leading to a decrease in the measured transmitted light energy and OL effects occur. Therefore, it is very interesting that despite the smaller contribution from NLS, the OL effect of CQD/GO hybrid was larger than that of the GO at the same linear transmittance at 532 nm.

Recently, the NLO and OL actions of graphene and graphene-based hybrids, including graphene, GO, metal/metal oxide–GO, semiconductor QD–GO, and hexagonal boron nitride nanosheets–graphene oxide (hBN-GO) nanocomposites, etc., have attracted considerable attention and increasing efforts have been attempted to explore their application in nonlinear optics field.[47–52] For example, enhanced two photon absorption properties of GO–Ag nanocomposite in comparison to those of GO under the excitation of a ns pulsed visible laser radiation of 532 nm wavelength were reported, and the extracted values of 2 PA β for GO–Ag is 45.4 cm GW^{-1} at a intensity of 0.2 GM cm^{-2}.[49] For graphene–ZnO, the 2 TA coefficient β is calculated to be -78.6×10^{-3} cm GW^{-1} at 18.7 GW cm^{-2} by 1030 nm and 340 fs laser exciting.[50] The obtained β values of CuO/functionalized hydrogen exfoliated graphene (f-HEG) hybrids with linear transmittance of 70% are of the order of 10^{-10} m W^{-1} while irradiated using 5 ns duration laser pulse at 532 nm.[51] Meanwhile, the 2 TA coefficient β of hexagonal boron nitride nanosheets–graphene oxide (BNNS–GO) heterostructure (0.1 mg mL^{-1}) is 14.3 cm GW^{-1} at 532 nm laser excitation.[52] The above results strongly suggested that the calculated nonlinear absorption coefficient of materials significantly depends on the measured conditions in the different labs, such as wavelength and pulse duration of excited laser, excited intensity, concentrations/linear transmittance of samples, and solvent, etc.

Despite of such confused situation, to explore the practical application of CQD/GO hybrid, it is helpful to compare the NLO and OL activities of CQD/GO hybrid with some of the reported work carried out under the similar measured condition with our group. It may be noted that the ns OL limiting threshold values of the CQD/GO hybrid is better than those of reported graphene-based nanostructures like graphene oxide nanosheets (>3 J cm^{-2}),[48] CuO/f-HEG hybrids (4.35 J cm^{-2}),[51] GO–Ag composites (6.4 J cm^{-2})[49] and comparable to benchmark materials like C60 (2 J cm^{-2})[53] and carbon black (2.2 J cm^2),[53] making CQD/GO hybrid attractive candidate for applications in eye and sensor protection from hazardous laser radiation. Furthermore, in Feng's study, they investigated the NLO properties and OL action of various GO nanostructures and among them graphene oxide nanosheets (GONs) and graphene oxide nanoribbons (GONRs), using 8 ns, 532 and 1064 nm laser pulses, the nonlinear absorption coefficient β of GONs has been determined to be 0.29×10^{-13} and 0.12×10^{-13} cm W^{-1} for visible and infrared laser pulses, respectively, while the corresponding values for GONRs were found to be 1.09×10^{-13} and 1.40×10^{-13} cm W^{-1}.[49] The nonlinear extinction coefficient of CQD/GO hybrid in the ns excitation regime improves two orders of magnitude as compared to Feng's reports. Such improvement nonlinear behavior strongly suggests that CQD/GO hybrids are highly promising for building photonic logic devices.

4. Conclusion

In summary, we have developed a one-step facile electrochemical method to synthesize novel CQD/GO nanocomposites that combine the advantages of both CQDs and GO. Based on the results obtained using TEM, Raman spectroscopy, and UV-vis spectroscopy, uniform decoration of CQDs on the two-dimensional GO surface was achieved. The linear optical properties of the as-prepared CQD/GO hybrid were studied by UV-vis absorption and PL spectroscopy. In this hybrid nanostructure, the luminescence of photoexcited CQDs is significantly quenched, possibly by a charge/energy transfer process from the CQDs to the GO, resulting in enhanced blue fluorescence from the GO. The NLO and OL performances were investigated by the open-aperture Z-scan technique in the nanosecond regime using a laser with a wavelength of 532 nm. The as-prepared CQD/GO composite offers a significantly improved OL performance compared with either GO or CQDs because of the charge/energy transfer process between the CQDs and GO. In addition, the OL threshold of CQD/GO hybrid is better than those of reported graphene-based nanostructures like GONs, CuO/f-HEG hybrids, GO–Ag composites and comparable to benchmark materials like C60 and carbon black and the value of β improves two orders of magnitude as compared to GONs and GONRs. The main contributors to the enhanced OL effect in the CQD/GO hybrid are a combination of nonlinear scattering and increased nonlinear absorption resulting from efficient charge/energy transfer at the CQD/GO interface.

Conflicts of interest

There are no conflicts to declare.

Acknowledgements

References

1 L. W. Tutt and T. F. Bogges, A Review Of Optical Limiting Mechanisms and Devices Semiconductors and Other Materials, *Prog. Quantum Electron.*, 1993, **17**, 299–338.

2 F. Wang, A. G. Gozhin, V. Scardaci, Z. Sun, F. Hennrich, I. H. White and A. C. Ferrari, Wideband-Tuneable, Nanotube Mode-Locked, Fibre Laser, *Nat. Nanotechnol.*, 2008, **3**, 738–742.

3 C. W. Spangler, Recent Development in the Design of Organic Materials for Optical Power Limiting, *J. Mater. Chem.*, 1999, **9**, 2013–2020.

4 C. Cocchi, D. Prezzi, A. Ruini, E. Molinari and C. Rozzi, Ab Initio Simulation of Optical Limiting: The Case of Metal-Free Phthalocyanine, *Phys. Rev. Lett.*, 2014, **112**, 198303.

5 K. E. Sekhosana, E. Amuhaya and T. Nyokong, Nanosecond Nonlinear Optical Limiting Properties of New Trinuclear Lanthanide Phthalocyanines in Solution and as Thin Films, *Polyhedron*, 2015, **85**, 347–354.

6 K. Sendhil, C. Vijayan and M. P. Kothiyal, Low-threshold Optical Power Limiting of Cw Laser Illumination Based on Nonlinear Refraction in Zinc Tetraphenyl Porphyrin, *Opt. Laser Technol.*, 2006, **38**, 512–515.

7 M. O. Senge, M. Fazekas, E. G. A. Notatras, W. J. Blau, M. Zawadzka, O. B. Locos and E. M. Ni Mhuircheartaigh, Nonlinear Optical Properties of Porphyrins, *Adv. Mater.*, 2007, **19**, 2737–2744.

8 S. Kang, J. Zhang, L. W. Sang, L. K. Shrestha, Z. Zhang, P. Lu, F. Li, M. Li and K. Ariga, Electrochemically Organized Isolated Fullerene-Rich Thin Films with Optical Limiting Properties, *ACS Appl. Mater. Interfaces*, 2016, **8**, 24295–24299.

9 X.-L. Zhang, Z.-B. Liu, X.-Q. Yan, X.-C. Li, Y.-S. Chen and J.-G. Tian, Nonlinear Optical and Optical Limiting Properties of Fullerene, Multi-walled Carbon Nanotubes, Graphene and Their Derivatives with Oxygen-Containing Functional Groups, *J. Opt.*, 2015, **17**, 015501.

10 P. Chen, X. Wu, X. Sun, J. Lin, W. Ji and K. L. Tan, Electronic Structure and Optical Limiting Behavior of Carbon Nanotubes, *Phys. Rev. Lett.*, 1999, **82**, 2548–2551.

11 Y. Chen, Y. Lin, Y. Liu, J. Doyle, N. He, X. D. Zhuang, J. R. Bai and W. J. Blau, Carbon Nanotube-Based Functional Materials for Optical Limiting, *J. Nanosci. Nanotechnol.*, 2007, **7**, 1268–1283.

12 J. Wang, Y. Chen and W. J. Blau, Carbon Nanotubes and Nanotube Composites for Nonlinear Optical Devices, *J. Mater. Chem.*, 2009, **19**, 7425–7443.

13 P. Chantharasupawong, R. Philip, N. T. Narayan, P. M. Sudeep, A. Mathkar, P. M. Ajayan and J. Thomas, Optical Power Limiting in Fluorinated Graphene Oxide: An Insight into the Nonlinear Optical Properties, *J. Phys. Chem. C*, 2012, **116**, 25955–25961.

14 Q. L. Bao, J. Q. Chen, Y. J. Xiang, K. Zhang, S. J. Li, X. F. Jiang, Q.-H. Xu, K. P. Loh and T. Venkatesan, Graphene Nanobubbles: A New Optical Nonlinear Material, *Adv. Opt. Mater.*, 2015, **3**, 744–749.

15 J. Wang, Y. Hernandez, M. Lotya, J. N. Coleman and W. J. Blau, Broadband Nonlinear Optical Response of Graphene Dispersions, *Adv. Mater.*, 2009, **21**, 2430–2435.

16 Y. J. Zhang, Y. Jin, M. L. He, L. Zhou, T. Xu, R. R. Yuan, S. Lin, W. D. Xiang and X. J. Liang, Optical Properties of Bimetallic Au–Cu Nanocrystals Embedded in Glass, *Mater. Res. Bull.*, 2018, **98**, 94–102.

17 Y.-X. Zhuang and Y.-H. Wang, Nonlinear Optical Properties of Metal Nanoparticles: A Review, *RSC Adv.*, 2017, **7**, 45129–45144.

18 K. B. Bhavitha, A. K. Nair, S. Perumbilavil, S. Jeseph, M. S. Kala, A. Saha, R. A. Narayanan, N. Hameed, S. Thomas and O. S. Oluwafemi, Investigating Solvent Effects on Aggregation Behaviour, Linear and Nonlinear Optical Properties of Silver Nanoclusters, *Opt. Mater.*, 2017, **73**, 695–705.

19 L.-B. Fang, W. Pan, S.-H. Zhong and W.-Z. Shen, Nonresonant and Resonant Nonlinear Absorption of CdSe-Based Nanoplatelets, *Chin. Phys. Lett.*, 2017, **34**, 098101.

20 S. Mathew, B. Samuel, A. Mujeeb, M. Kailasnath, V. P. N. Nampoori and C. P. Girijavallabhan, Effect of Au Coating on Optical Properties of CdS Nanoparticles and Their Optical Limiting Studies, *Opt. Mater.*, 2017, **72**, 673–679.

21 J. V. Antony, J. J. Pillai, P. Kurian, V. P. N. Nampoori and G. E. Kochimoolayil, Photoluminescence and Optical Nonlinearity of CdS Quantum Dots Synthesized in a Functional Copolymer Hydrogel Template, *New J. Chem.*, 2017, **41**, 3524–3536.

22 K. Sanusi, E. K. Amuhaya and T. Nyokong, Enhanced Optical Limiting Behavior of an Indium Phthalocyanine–Single-Walled Carbon Nanotube Composite: An Investigation of the Effects of Solvents, *J. Phys. Chem. C*, 2014, **118**, 7057–7069.

23 X.-L. Zhang, Z.-B. Liu, X. Zhao, X.-Q. Yan, X. C. Li and J.-G. Tian, Optical Limiting Effect and Ultrafast Saturable Absorption in a Solid PMMA Composite Containing Porphyrin-Covalently Functionalized Multi-Walled Carbon Nanotubes, *Opt. Express*, 2013, **21**, 25277–25284.

24 B. Anand, A. Kaniyoor, S. S. S. Sai, R. Philip and S. Ramaprabhu, Enhanced Optical Limiting in Functionalized Hydrogen Exfoliated Graphene and its Metal Hybrids, *J. Mater. Chem. C*, 2013, **1**, 2773–2780.

25 A. J. Wang, W. Yu, Y. Fang, Y. L. Song, D. Jia, L. L. Long, M. P. Cifuentes, M. G. Humphrey and C. Zhang, Facile Hydrothermal Synthesis and Optical Limiting Properties of TiO$_2$-Reduced Graphene Oxide Nanocomposites, *Carbon*, 2015, **89**, 130–141.

26 Q. Y. Ouyang, H. L. Yu, Z. Xu, Y. Zhang, C. Y. Li, L. H. Qi and Y. J. Chen, Synthesis and Enhanced Nonlinear Optical Properties of Graphene/CdS Organic Glass, *Appl. Phys. Lett.*, 2013, **102**, 031912.

27 W. N. Song, C. Y. He, W. Zhang, Y. C. Gao, Y. X. Yang, Y. Q. Wu, Z. M. Chen, X. C. Li and Y. L. Dong, Synthesis and Nonlinear Optical Properties of Reduced Graphene Oxide Hybrid Material Covalently Functionalized With Zinc Phthalocyanine, *Carbon*, 2014, **77**, 1020–1030.

28 Y. L. Du, N. N. Dong, M. H. Zhang, K. Zhu, R. Q. Na, S. L. Zhang, N. W. Sun, G. B. Wang and J. Wang, Covalent Functionalization of Graphene Oxide with Porphyrin and Porphyrin Incorporated Polymers for Optical Limiting, *Phys. Chem. Chem. Phys.*, 2017, **19**, 2252–2260.

29 O. C. Compton and S. B. T. Nguyen, Graphene Oxide, Highly Reduced Graphene Oxide, and Graphene: Versatile Building Blocks for Carbon-Based Materials, *Small*, 2010, **6**, 711–723.

30 K. P. Loh, Q. L. Bao, P. K. Ang and J. X. Yang, The Chemistry of Graphene, *J. Mater. Chem.*, 2010, **20**, 2277–2289.

31 Q. Tang, Z. Zhou and Z. F. Chen, Graphene-Related Nanomaterials: Tuning Properties by Functionalization, *Nanoscale*, 2013, **5**, 4541–4583.

32 Y. F. Wang and A. G. Hu, Carbon Quantum Dots: Synthesis, Properties and Applications, *J. Mater. Chem. C*, 2014, **2**, 6921–6939.

33 S. Y. Lim, W. Shen and Z. Q. Gao, Carbon Quantum Dots and Their Applications, *Chem. Soc. Rev.*, 2015, **44**, 362–381.

34 P. G. Luo, S. Sahu, S.-T. Yang, S. K. Sonkar, J. P. Wang, H. F. Wang, G. E. LeCroy, L. Cao and Y.-P. Sun, Carbon "Quantum" Dots for Optical Bioimaging, *J. Mater. Chem. B*, 2013, **1**, 2116–2127.

35 D. Z. Tan, Y. Y. Yamada, S. F. Zhou, Y. Shimotsuma, K. Miura and J. R. Qiu, Carbon Nanodots With Strong Nonlinear Optical Response, *Carbon*, 2014, **69**, 638–640.

36 I. Papagiannouli, A. B. Bourlinos, A. Bakandristsos and S. Couris, Nonlinear Optical Properties of Colloidal Carbon Nanoparticles: Nanodiamonds and Carbon Dots, *RSC Adv.*, 2014, **4**, 40152–40160.

37 A. B. Bourlinos, M. A. Karakassides, A. Kouloumpis, D. Gournis, A. Bakandritsos, I. Papagiannouli, P. Aloukos, S. Couris, K. Hola, R. Zboril, M. Krysmann and E. P. Giannelis, Synthesis, Characterization and Non-Linear Optical Response of Organophilic Carbon Dots, *Carbon*, 2013, **61**, 640–643.

38 P. Aloukos, I. Papagiannouli, A. B. Bourlinos, R. Zboril and S. Couris, Third-Order Nonlinear Optical Response and Optical Limiting of Colloidal Carbon Dots, *Opt. Express*, 2014, **22**, 12013–12027.

39 M. Qi, L. Bai, H. Y. Xu, Z. Q. Wang, Z. H. Kang, X. N. Zhao, W. Z. Liu, J. G. Ma and Y. C. Liu, Oxidized carbon quantum dot–graphene oxide nanocomposites for improving data retention of resistive switching memory, *J. Mater. Chem. C*, 2018, **6**, 2026–2033.

40 W. S. Hummers and R. E. Offeman, Preparation of Graphitic Oxide, *J. Am. Chem. Soc.*, 1958, **80**, 1339.

41 M. Sheik-Bahae, A. A. Said, T.-H. Wei, D. J. Hagan and E. W. V. Stryland, Sensitive Measurement of Optical Nonlinearities Using a Single Beam, *IEEE J. Quantum Electron.*, 1990, **26**, 760–769.

42 A. Pramanik, A. K. Kole, R. N. Krishnaraj, S. Biswas, C. S. Tiwary, P. Varalakshmi, S. K. Rai, B. A. Kumar and P. Kumbhakar, A Novel Technique of Synthesis of Highly Fluorescent Carbon Nanoparticles from Broth Constituent and In vivo Bioimaging of *C. elegans*, *J. Fluoresc.*, 2016, **26**, 1541–1548.

43 S. J. Zhu, Y. B. Song, X. H. Zhao, J. R. Shao, J. H. Zhang and B. Yang, The Photoluminescence Mechanism in Carbon Dots (Graphene Quantum Dots, Carbon Nanodots, and Polymer Dots): Current State and Future Perspective, *Nano Res.*, 2015, **8**, 355–381.

44 L. Wang, S.-J. Zhu, H.-Y. Wang, S.-N. Qu, Y.-L. Zhang, J.-H. Zhang, Q.-D. Chen, H.-L. Xu, W. Han, B. Yang and H.-B. Sun, Common Origin of Green Luminescence in Carbon Nanodots and Graphene Quantum Dots, *ACS Nano*, 2014, **8**, 2541–2547.

45 V. Joudrier, P. Bourdon, F. Hache and C. Flytzanis, Nonlinear Light Scattering in a Two-Component Medium: Optical Limiting Application, *Appl. Phys. B: Lasers Opt.*, 1998, **67**, 627–632.

46 S. Sivaramakrishnan, V. S. Muthukumar, S. S. Sai, K. Venkataramaniah, J. Reppert, A. M. Rao, M. Anija, R. Philip and N. Kuthirummal, Nonlinear Optical

Scattering and Absorption in Bismuth Nanorod Suspensions, *Appl. Phys. Lett.*, 2007, **91**, 093104.

47 N. Liaros, P. Aloukos, A. Kolokithas-Ntoukas, A. Bakandritsos, T. Szabo, R. Zboril and S. Couris, Nonlinear Optical Properties and Broadband Optical Power Limiting Action of Graphene Oxide Colloids, *J. Phys. Chem. C*, 2013, **117**, 6842–6850.

48 M. Feng, H. B. Zhan and Y. Chen, Nonlinear optical and optical limiting properties of graphene families, *Appl. Phys. Lett.*, 2010, **96**, 033107.

49 S. Biswas, A. K. Kole, C. S. Tiwary and P. Kumbhakar, Enhanced nonlinear optical properties of graphene oxide–silver nanocomposites measured by *Z*-scan technique, *RSC Adv.*, 2016, **6**, 10319–10325.

50 Q. Tong, Y.-H. Wang, X.-X. Yu, B. Wang, Z. Liang, M. Tang, A.-S. Wu, H.-J. Zhang, F. Liang, Y.-F. Xie and J. Wang,

Nonlinear optical and multi-photon absorption properties in graphene ZnO nanocomposites, *Nanotechnology*, 2018, **29**, 165706.

51 B. Anand, A. Kaniyoor, D. Swain, T. T. Baby, S. V. Rao, S. S. Sai, S. Ramaprabhub and R. Philip, Enhanced optical limiting and carrier dynamics in metal oxide-hydrogen exfoliated graphene hybrids, *J. Mater. Chem. C*, 2014, **2**, 10116–10123.

52 S. Biswas, C. S. Tiwary, S. Vinod, A. K. Kole, U. Chatterjee, P. Kumbhakar and P. M. Ajayan, Nonlinear Optical Properties and Temperature Dependent Photoluminescence in hBN-GO Heterostructure 2D Material, *J. Phys. Chem. C*, 2017, **121**, 8060–8069.

53 P. Chen, X. Wu, X. Sun, J. Lin, W. Ji and K. L. Tan, Electronic structure and optical limiting behavior of carbon nanotubes, *Phys. Rev. Lett.*, 1999, **82**, 2548.